JGR Oceans

RESEARCH ARTICLE
10.1029/2018JC014923

Special Section:
Forum for Arctic Modeling and Observational Synthesis (FAMOS) 2: Beaufort Gyre phenomenon

Arctic Ocean Freshwater Dynamics: Transient Response to Increasing River Runoff and Precipitation

Nicola Jane Brown[1], **Johan Nilsson**[2], **and Per Pemberton**[3]

[1]Ocean and Earth Science, University of Southampton, Southampton, UK, [2]Department of Meteorology, Stockholm University, Stockholm, Sweden, [3]Oceanographic Research Unit, Swedish Meteorological and Hydrological Institute, Gothenburg, Sweden

Key Points:
- Response of freshwater content to change in freshwater input approximated by a response function with *e*-folding time scale of about 10 years
- Detail of the response depends on the source of freshwater input and its associated spatial anomalies, which introduce secondary time scales
- Response for precipitation is more complex than for river runoff because of a more complex footprint that also influences net sea ice growth

Correspondence to:
N. J. Brown,
N.J.Brown@soton.ac.uk

Citation:
Brown, N. J., Nilsson, J., & Pemberton, P. (2019). Arctic Ocean freshwater dynamics: Transient response to increasing river runoff and precipitation. *Journal of Geophysical Research: Oceans*, *124*, 5205–5219. https://doi.org/10.1029/2018JC014923

Received 28 DEC 2018
Accepted 15 JUN 2019
Accepted article online 21 JUN 2019
Published online 25 JUL 2019

Abstract Simulations from a coupled ice-ocean general circulation model are used to assess the effects on Arctic Ocean freshwater storage of changes in freshwater input through river runoff and precipitation. We employ the climate response function framework to examine responses of freshwater content to abrupt changes in freshwater input. To the lowest order, the response of ocean freshwater content is linear, with an adjustment time scale of approximately 10 years, indicating that anomalies in Arctic Ocean freshwater export are proportional to anomalies in freshwater content. However, the details of the transient response of the ocean depend on the source of freshwater input. An increase in river runoff results in a fairly smooth response in freshwater storage consistent with an essentially linear relation between total freshwater content and discharge of excess freshwater through the main export straits. However, the response to a change in precipitation is subject to greater complexity, which can be explained by the localized formation and subsequent export of salinity anomalies which introduce additional response time scales. The results presented here suggest that future increases in Arctic Ocean freshwater input in the form of precipitation are more likely to be associated with variability in the storage and release of excess freshwater than are increases in freshwater input from river runoff.

Plain Language Summary This paper shows that the Arctic Ocean adjusts to changes in freshwater input over time scales of about one decade. How much of the added freshwater is stored in the Arctic depends, however, on how the freshwater enters the ocean. If it arrives as additional river runoff, the response in Arctic freshwater storage is relatively smooth and predictable. If it falls, instead, as increased precipitation, the response is less easy to predict because it is complicated by interactions between the ocean and sea ice. This is important because the part of the freshwater that is not stored in the Arctic Ocean is exported to the North Atlantic, where it can affect the global ocean circulation.

1. Introduction

The Arctic Ocean has a major influence on global circulation through the provision of dense waters to supply deep convection in the Nordic and Labrador seas (Yang et al., 2016). The net effect of the Arctic is to cool and freshen relatively warm, saline water flowing in via the Fram Strait or Barents Sea from the Atlantic (Rudels et al., 2013), before it returns southward either through the Fram Strait or the Canadian Arctic Archipelago (CAA). Some water returns denser than it entered, some lighter, a two-fold influence that has been described as driving a double estuarine circulation (Eldevik & Nilsen, 2013).

Densification of inflowing Atlantic Water occurs mainly through surface heat loss in the Barents Sea (Rudels, 2010). Across most of the rest of the Arctic Ocean, the Atlantic Water layer is overlain by a lighter, fresher surface layer, formed through the influx of freshwater. The largest source of freshwater input is runoff from rivers around the continental margins of Siberia and North America, amounting to ~4,200 km^3/year during the period 2000–2010. Net precipitation contributes a further ~2200 km^3/year (Haine et al., 2015). The inflow of Pacific Water through the Bering Strait also serves as a source of freshwater, since its salinity is lower than that of Atlantic Water; it contributed ~2,600 km^3/year with respect to a reference salinity of 34.80 in 2000–2010 (Haine et al., 2015; Woodgate et al., 2005).

Sources and sinks of freshwater are not typically in constant balance, and the proportion of freshwater input retained within the Arctic Ocean rather than being exported directly varies on time scales of O(1–10) years

(Proshutinsky et al., 2009). This periodic storage and release has been linked to variation in circulation driven by cyclical changes in wind patterns both in the Beaufort Sea region and across the Siberian shelves (Haine et al., 2015; Morison et al., 2012; Polyakov et al., 2008). More generally, Johnson et al. (2018) find that the variability of Arctic freshwater content (FWC) in recent years can be explained chiefly by the influence of sea level pressure variations on sources, sinks, and storage of freshwater. Proshutinsky et al. (2009) note that the range of variation of freshwater storage has increased since 2003 and suggest that it could continue to do so as climate change intensifies.

The warming global climate is also driving increasing freshwater input to the Arctic Ocean (Bintanja & Selten, 2014; Vavrus et al., 2012). River runoff is projected to reach 5,500 km^3/year and net precipitation 2,500 km^3/year by 2100 (Haine et al., 2015), and increases in Pacific Water inflow are also expected. While the influence of wind patterns on freshwater storage has benefitted from much recent investigation, the role of freshwater as a modifier of ocean circulation in its own right, rather than as a passive tracer of wind-driven currents, has received less attention. As Morison et al. (2012) observed, variation in the wind-driven Ekman pumping over the Beaufort Gyre region might be the main factor controlling the freshwater storage in the Gyre, but additional processes such as baroclinic eddies and mechanical ice-ocean feedbacks (Dewey et al., 2018; Manucharyan & Spall, 2016; Meneghello et al., 2017) influence the FWC of the Gyre.

A steady-state modeling study by Pemberton and Nilsson (2016) showed that increased freshwater supply from runoff and precipitation results in a weakening of the Beaufort Gyre and a redirection of some freshwater export from the CAA to the Fram Strait. Nummelin et al. (2016) found a similar weakening of the anticyclonic surface circulation in simulations of increased runoff while noting also that the strengthening of the Arctic Ocean stratification caused by the increased freshwater input leads to a reduction in the transfer of anticyclonic atmospheric momentum to the Atlantic Water layer below the halocline and thus a strengthening of the cyclonic Atlantic Water circulation. Increased runoff has also been shown (Lambert et al., 2019) to affect various processes associated with the diffusion of heat and salt, leading ultimately to an increase in the advective heat and salt import into the Arctic. Given the influence that increasing freshwater input appears to have on circulation patterns, there is a need for an improved understanding of the effect that enhanced freshwater input is likely to have on Arctic storage of freshwater and its release to the north Atlantic.

Previous studies have considered the long-term response of the ocean to changes in forcing. For that reason, we focus here on the transient response: We draw on the "climate response function" (CRF) framework described by Marshall et al. (2017), using simulations from a coupled ice-ocean general circulation model (GCM) to investigate the relationship between changes in freshwater input to the ocean and the response of the ocean in terms of storage and export of freshwater. The rationale for the CRF methodology is that if the transient response (the CRF) of an observable to step function forcing is known, the CRF may then be convolved with any more realistic time history of forcing to determine a predicted linear response for that observable. Note that the CRF is convolved with the time derivative of the forcing (Marshall et al., 2017). The impulse response function, which is the time derivative of the CRF, is convolved with the forcing itself to give the response. We take as our observables here the FWC of the Arctic Ocean in liquid and sea ice form and the export of freshwater through key straits. We apply step change perturbations to the freshwater input from river runoff and precipitation to examine the time scales, pathways, and mechanisms governing the likely response of the ocean to changes in freshwater input.

2. Method and Theoretical Background

2.1. General Circulation Model

In this study we have used a coupled ice-ocean model, the Massachusetts Institute of Technology general circulation model (MITgcm), in a regional configuration covering the Arctic Ocean and parts of the North Atlantic and North Pacific oceans north of ~ 55°N. This model setup has been used in a number of previous studies (e.g., Condron et al., 2009; Manizza et al., 2009; Nguyen et al., 2011), and Condron et al. (2009) showed that it reasonably reproduces the Arctic Ocean freshwater budget. The horizontal grid spacing within the model domain (see Figure 1) is ~18 km, and the model grid has 50 vertical layers with thickness ranging from 10 m at the surface to ~450 m for the deepest layer. Further details of the model setup are

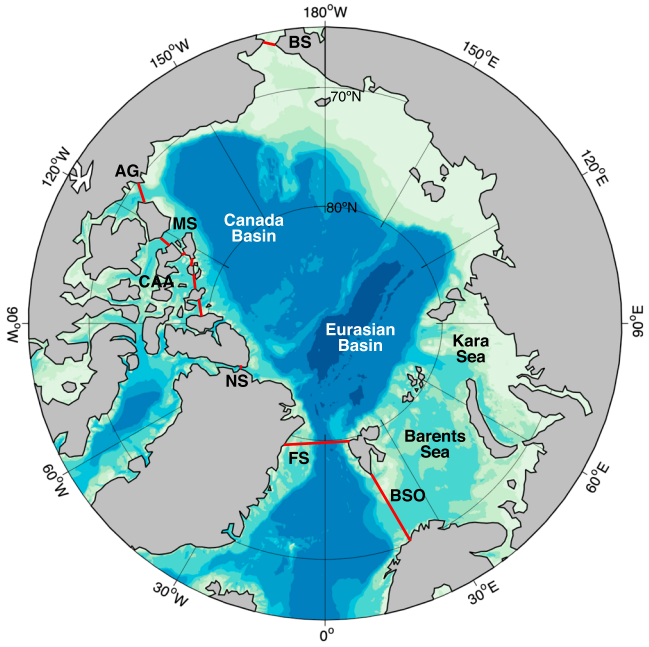

Figure 1. The boundaries of the model domain within which perturbations of surface freshwater input were made are indicated by red lines. The shading shows bathymetry. AG = Amundsen Gulf; MS = McClure Strait; CAA = Canadian Arctic Archipelago; NS = Nares Strait; FS = Fram Strait; BSO = Barents Sea Opening).

given in Pemberton and Nilsson (2016), and the model parameters employed are as described in Nguyen et al. (2011).

2.2. Model Simulations

Ocean forcing for the majority of the simulations described here was provided by the Japanese 25-year Reanalysis (JRA-25; Onogi et al., 2007), which covers the period 1979–2004, extended for a further 9 years to 2013 using operational analysis from the same model system. For a small number of additional simulations, the model was instead forced with a repeating annual cycle of atmospheric forcing (the Coordinated Ocean-Ice Reference Experiments (CORE) II corrected normal year forcing; Griffies et al., 2009). For river runoff data, we used a monthly climatology derived from Arctic Runoff Database raw data and adjusted to account for ungauged river flows, as described in Nguyen et al. (2011). The model was initialized for each simulation using sea ice conditions from the Polar Science Center (Zhang & Rothrock, 2003) and ocean conditions from the World Ocean Atlas 2005 (Antonov et al., 2006; Locarnini et al., 2006).

The model was first run for 35 years in a control simulation, using the forcing described above to represent the state of the Arctic in the late twentieth century. To test the response of the ocean to an abrupt change in freshwater input, further simulations were then run in which river runoff or precipitation was increased or decreased by a fixed proportion (−30% to +100% for runoff and −30% or +30% for precipitation) of the control forcing for the duration of the simulation. The larger increases are greater than those expected to be seen in the real future Arctic but were included in the suite of simulations to test the linearity of the response. Evaporation and sea ice formation and melt were not perturbed directly through forcing but evolved during the simulations in response to the perturbation of runoff or precipitation.

For each simulation, monthly means of freshwater height (H_F) and liquid FWC (V_F) were calculated:

$$H_F(x, y, t) = \int_{-H_0}^{0} \frac{S_{ref} - S(x, y, z, t)}{S_{ref}} \, dz, \tag{1}$$

$$V_F(t) = \int_A H_F(x, y, t) \, dA, \tag{2}$$

where z is depth, S salinity, and A the horizontal area of the basin. The reference salinity, S_{ref}, was taken to be 35.0 g/kg. The integrations were performed to a depth $-H_0$ of −277 m, indicative of the upper surface of the Atlantic Water layer. Where storage of freshwater in sea ice is discussed, an equivalent FWC has been calculated from stored sea ice volumes assuming a sea ice density of 900 kg/m^3 and salinity of 6.0 g/kg.

2.3. A Conceptual Model for Rotationally Controlled Export

We have compared the ocean freshwater response in the model simulations described above to theoretical predictions given by a simple conceptual model such as described by Stigebrandt (1981), Nilsson and Walin (2010), and Rudels (2010). A key issue is whether the CRF to perturbations in freshwater input will, to the lowest order, depend only on the anomaly of the total FWC, as assumed in the conceptual model, or if spatial variations matter. Further, is the response independent of wind-forcing regimes over the Arctic Ocean?

The version of the conceptual model that we have adopted here represents the Arctic Ocean as stratified by salinity into two layers separated by a halocline at constant depth H: a fresher, upper layer of salinity S_1 above the halocline and a layer of Atlantic Water with salinity S_A below. In the model, the freshwater export depends on the net Arctic FWC and a simple representation of wind forcing in the basin. The final result is a further simplified linearized model, in which perturbations in freshwater export and net content are linearly related. Despite these simplifications, the model yields a leading-order description of how the net Arctic Ocean FWC in the ocean circulation model responds to changes in the freshwater input, as will be shown below.

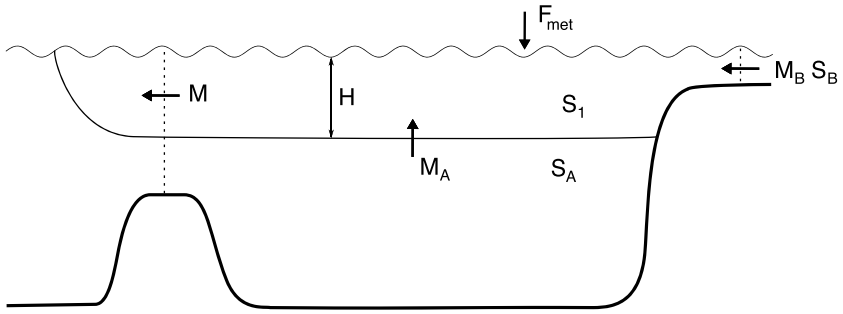

Figure 2. Sketch of the two-layer conceptual model. H is the depth of the halocline separating the two layers, S_A the salinity of the lower layer, and S_1 the salinity of the upper layer. M_B is the volume flux of water entering through the Bering Strait and S_B its salinity. F_{met} is the influx of meteoric freshwater from river runoff and net precipitation, M_A the volume flux of water entrained from the lower layer to the upper by mixing, and M the volume flux of outflow.

A schematic diagram of the model appears as Figure 2. The outflow from the upper layer of the basin is represented by a volume flux M. A flux F_{met} of freshwater enters the upper layer through river runoff or net precipitation (precipitation minus evaporation), and a flux M_B of Pacific Water of salinity S_B enters through the Bering Strait. A flux M_A of Atlantic Water is entrained into the upper layer from below by mixing. The horizontal surface area of the basin is A.

The volume budget for the upper layer is

$$A\frac{dH}{dt} = -M + M_A + M_B + F_{met}, \tag{3}$$

while the salinity budget is

$$A\frac{d(S_1 H)}{dt} = -MS_1 + M_A S_A + M_B S_B. \tag{4}$$

By dividing equation (4) by S_A, which we assume to be constant, and subtracting from equation (3), we obtain

$$A\frac{dH_F}{dt} = -M\frac{\Delta S}{S_A} + M_B\left(1 - \frac{S_B}{S_A}\right) + F_{met}, \tag{5}$$

where $\Delta S \equiv S_A - S_1$ and freshwater height is defined by analogy with equation (1) as $H_F \equiv \left(\frac{S_A - S_1}{S_A}\right)H$.

Following Stigebrandt (1981), we assume that the outflow from the Arctic Ocean is in geostrophic balance and occurs in an exit strait that is wide compared to the first Rossby radius. This allows us to write the outflow as

$$M = M_G + M_W. \tag{6}$$

Here the baroclinic geostrophic transport component is given by

$$M_G = \frac{\beta \Delta S g H^2}{2f}, \tag{7}$$

where β is the haline expansion coefficient, g the acceleration due to gravity, and f the Coriolis parameter. We have ignored any density difference due to difference in the temperatures of inflowing Atlantic Water and outflow water: Assuming a temperature and salinity of 6 °C and 35.0 g/kg, respectively, for inflowing water and −1 °C and 31.0 g/kg for outflowing water, the contribution of salinity to density difference is about 5 times that of temperature. Further, we have included a barotropic, wind-forced transport component given by

$$M_W = v(t)LH, \tag{8}$$

where $v(t)$ is wind-driven velocity and L the cross-stream width of the flow in the exit strait. One interpretation of M_W is that it represents the additional transport to M_G due to a barotropic velocity v in the lower layer that extends throughout the upper layer (Pemberton & Nilsson, 2016). If $v = 0$ and the lower layer is

at rest, then the outflow is given solely by the baroclinic component M_G. A more general view is that $v(t)$ reflects how wind forcing over the basin influences the outflow and storage of freshwater. In periods with more cyclonic wind forcing over the Arctic Ocean, the FWC tends to decrease and vice versa (Haine et al., 2015). Crudely, the effect of changing wind forcing can be represented by making $v(t)$ larger for cyclonic wind regimes and smaller for anticyclonic regimes. We write

$$v(t) = v_0 + \Delta v(t), \tag{9}$$

where v_0 is related to the long-term time mean winds and $\Delta v(t)$ to time-varying winds. Observations and modeling suggest that low-frequency wind variations over the Arctic Ocean result in relative changes in the FWC of some 10% to 20% (Haine et al., 2015; Johnson et al., 2018; Pemberton & Nilsson, 2016; Stewart & Haine, 2013). Accordingly, we expect that $|\Delta v(t)|/v(t)$ in this simple model should also be allowed to vary by about 10% to 20%, implying that $|\Delta v(t)|$ should be small compared to v_0. Substituting into equation (5) and defining $F \equiv M_B(1 - \frac{S_B}{S_A}) + F_{met}$ yields

$$A\frac{dH_F}{dt} = -\frac{\beta g S_A {H_F}^2}{2f} - v(t)LH_F + F. \tag{10}$$

Now consider the effect of a perturbation, ΔF, in freshwater input, leading to an anomaly, ΔH_F, in freshwater height. Equation (10) as applied to the perturbed state becomes

$$A\frac{d(H_F + \Delta H_F)}{dt} = -\frac{\beta g S_A (H_F + \Delta H_F)^2}{2f} - v(t)L(H_F + \Delta H_F) + F + \Delta F. \tag{11}$$

We assume that if the perturbation ΔF is small, the resultant anomaly will also be $H_F \gg \Delta H_F$, so that

$$(H_F + \Delta H_F)^2 \approx {H_F}^2 + 2H_F\Delta H_F. \tag{12}$$

Linearizing equation (11) accordingly and subtracting equation (10), we have

$$\frac{d\Delta H_F}{dt} = -\frac{\beta g S_A H_F \Delta H_F}{Af} - \frac{(v_0 + \Delta v(t))L\Delta H_F}{A} + \frac{\Delta F}{A}. \tag{13}$$

If we further assume that $v_0 \gg |\Delta v(t)|$, this equation simplifies to

$$\frac{d\Delta H_F}{dt} = -\tau^{-1}\Delta H_F + \frac{\Delta F}{A}, \tag{14}$$

where we have introduced the response time scale τ:

$$\tau \equiv \left(\frac{\beta g S_A H_F f^{-1} + v_0 L}{A}\right)^{-1}. \tag{15}$$

The (climate) response function to equation (14), describing the response to a step function freshwater perturbation (Marshall et al., 2017), is

$$CRF(t) = 1 - \exp(-t/\tau) \tag{16}$$

for $t \geq 0$ and 0 for $t < 0$. Thus, in this limit of weak wind variations (i.e., $v_0 \gg |\Delta v(t)|$), the conceptual model predicts an exponential adjustment of forced freshwater perturbations over a time scale that is essentially independent of the variations of the wind field. Note that the time scale depends on the background state freshwater height H_F, which according to equation (10) responds to wind variations represented by the term $\Delta v(t)$. As noted above, observed fractional changes of FWC on interannual to decadal scales, presumably driven by wind variations, are only about 10% to 20% (Haine et al., 2015; Morison et al., 2012). This suggests that in the present conceptual model, a climatological constant value of H_F can be used to approximate τ.

Next, we consider the time scale of the response function predicted by the conceptual model. In the limiting case when $v_0 = 0$, the response time scale defined by equation (17) is set by the geostrophic flow (Rudels, 2010):

$$\tau_G = \frac{Af}{\beta g S_A H_F}. \tag{17}$$

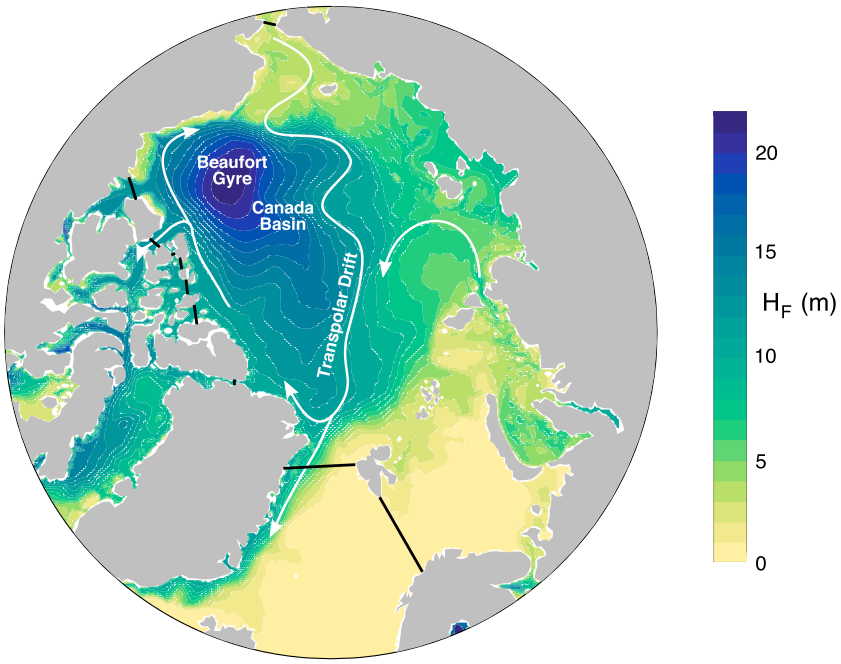

Figure 3. Time-mean freshwater height, H_{F}, in meters for the final decade of the reference simulation, integrated to a depth of −277 m, with $S_{\mathrm{ref}} = 35.0$ g/kg. White arrows indicate major currents in the upper 100 m.

Inserting typical values for the Arctic ($\beta = 8 \times 10^{-4}, f = 1.4 \times 10^{-4}\mathrm{s}^{-1}, A = 9 \times 10^{12}\mathrm{m}^2, g = 10\,\mathrm{m/s}^2, S_A = 35.0$ g/kg) into this expression and estimating H_{F} by dividing a freshwater volume of $8 \times 10^4\,\mathrm{km}^3$ from Pemberton and Nilsson (2016) by A give a predicted time scale of 16 years.

We may compare this predicted time scale with that implied by steady state in any system involving storage and flux, the ratio of the two giving a mean residence time. From the steady-state version of equation (10), still with $v = 0$, the geostrophic adjustment time scale in equation (17) may be written as

$$\tau_G = \frac{AH_{\mathrm{F}}}{2F} = \frac{1}{2} \times \frac{\text{Liquid FWC}}{\text{Net freshwater supply}}. \tag{18}$$

(The factor of a half derives from the assumption that outflow from the Arctic is governed by geostrophy.) An increase in H_{F} increases both the volume export and the salinity export anomaly, which yields a shorter τ. Adopting estimates of net freshwater input from meteoric sources and from Bering Strait inflow from Pemberton and Nilsson (2016) leads to an alternative predicted time scale of 12 years.

Equation (15) shows that τ decreases with the wind-related velocity v_0. In the limit when the geostrophic contribution becomes negligible compared to the wind-driven component, the steady-state version of equation (10) yields

$$\tau_{\mathrm{W}} = \frac{AH_{\mathrm{F}}}{F} = \frac{\text{Liquid FWC}}{\text{Net freshwater supply}}, \tag{19}$$

implying a predicted τ of 24 years if the same estimates of net freshwater input as for the case of geostrophic export are assumed. This confirms that τ in the conceptual model is proportional to the FWC divided by the net freshwater supply regardless of the relative magnitudes of the geostrophic transport M_{G} and the wind-driven transport M_{W}; however, the constant of proportionality varies depending on whether geostrophic or wind-driven transport dominates, being 1/2 for purely geostrophic flow and 1 for purely barotropic wind-driven flow.

We compare these predictions of the net FWC with the response seen in the experiments performed using the general circulation model and investigate neglected physics that might lead to any departure from the predictions of the conceptual model.

3. Results

Typical spatial variability in liquid FWC, V_F, can be seen in Figure 3, which shows mean depth-integrated freshwater height, H_F, for the final 10 years of the control simulation. The concentration of freshwater in the Canada Basin, and in particular in the region occupied by the Beaufort Gyre, is clearly visible.

3.1. Reference Simulation

The evolution of liquid FWC, V_F, for the reference simulation over the simulation period is shown in Figure 4a. Monthly mean V_F is denoted by the thinner line, while the heavier line represents a 12-month running mean. Annual mean volumes range from around 75×10^3 to 85×10^3 km^3 over the 35-year period. There is a marked seasonal cycle of amplitude around 7×10^3 km^3, or about 9% of the mean volume, with V_F reaching a seasonal maximum in September/October and minimum in May/June of each year; we attribute this to the seasonal storage of freshwater in sea ice.

As has been discussed briefly by Pemberton and Nilsson (2016), we also note significant variability in V_F over decadal scales. The annual mean volume is at the upper end of its range at the beginning of the simulation period and remains reasonably level for the first decade. It then falls by about 10×10^3 km^3 between years 10 and 18 (representing the period 1989 to 1997), accompanied by a decline in sea ice FWC (see Figure 5a). From year 18 to year 33 (1997 to 2012), a steady increase in V_F is seen, partially compensated by a continued fall in sea ice FWC. The pattern seen in the latter half of the simulation is consistent with an increase in Arctic Ocean liquid FWC seen in observations (Haine et al., 2015) since the 1990s. Rabe et al. (2011) accounted for an increase in the central Arctic basin through strengthened regional Ekman pumping lowering the lower halocline (as described by Proshutinsky et al., 2009) and freshening of the water above the halocline through sea ice melt, as we find in the current simulations. (Rabe et al., 2011, also discussed the advection of extra river water from the Siberian shelves to the deep Arctic Ocean, but the integrated V_F totals quoted here include the shelf areas, and so such a redistribution of freshwater does not affect them.)

We investigate the response of the ocean to changing freshwater input by running further simulations in which runoff or precipitation is increased or decreased by a fixed proportion of the control forcing. These changes are introduced without specifically addressing what atmospheric circulation regime changes or climate change patterns may cause the perturbations of the freshwater supply. Global warming, which amplifies the hydrological cycle and decreases the Arctic sea ice export (Haine et al., 2015; Held & Soden, 2006), can increase the freshwater input to the Arctic Ocean essentially without any change in the time-mean atmospheric circulation. Through natural variability, river runoff is observed to increase primarily under the atmospheric anticyclonic circulation regime, when trajectories of cyclones with moisture from the North Atlantic are shifted toward Siberia and runoff from Siberian rivers increases (Haine et al., 2015; Proshutinsky et al., 1999, 2015). Conversely, increased precipitation over the Arctic Ocean is expected primarily under cyclonic wind forcing regimes (Proshutinsky et al., 1999, 2015).

Rather than introducing combined step function changes in freshwater forcing and wind forcing consistent with the observed natural variability, we have performed freshwater perturbation experiments on a background forcing provided by the observationally based time-varying JRA-25 (Onogi et al., 2007). An underlying assumption is that, to the lowest order, the response to changes in freshwater input is controlled by the time-mean features of the Arctic atmosphere-ocean circulation and hence can be studied using CRFs specific to freshwater forcing. The linear response of the Arctic FWC to natural variability, or forced climate change, can in principle be described by convolutions of the time history of wind and freshwater forcing with their respective CRFs (Marshall et al., 2017). Hence, our simulations may reveal information on aspects of the CRFs for freshwater forcing that depend primarily on the time-mean state of the atmospheric circulation. To examine the sensitivity to variations in atmospheric forcing, we also briefly report the result of additional simulations forced with a repeating annual cycle of atmospheric forcing: the CORE-II corrected normal year forcing (Griffies et al., 2009). Here the freshwater perturbations in the simulations evolve under an atmospheric forcing without any interannual variations, which may help to reveal the sensitivity of the freshwater response to wind variations. Note that the freshwater inputs from river runoff and precipitation have seasonal cycles. Thus, in the simulations with step function increases of the freshwater inputs, there will be changes of both the time mean and seasonality of the freshwater forcing. As will be discussed below, however, the change of the time mean freshwater input tends to dominate the response of the FWC anomalies.

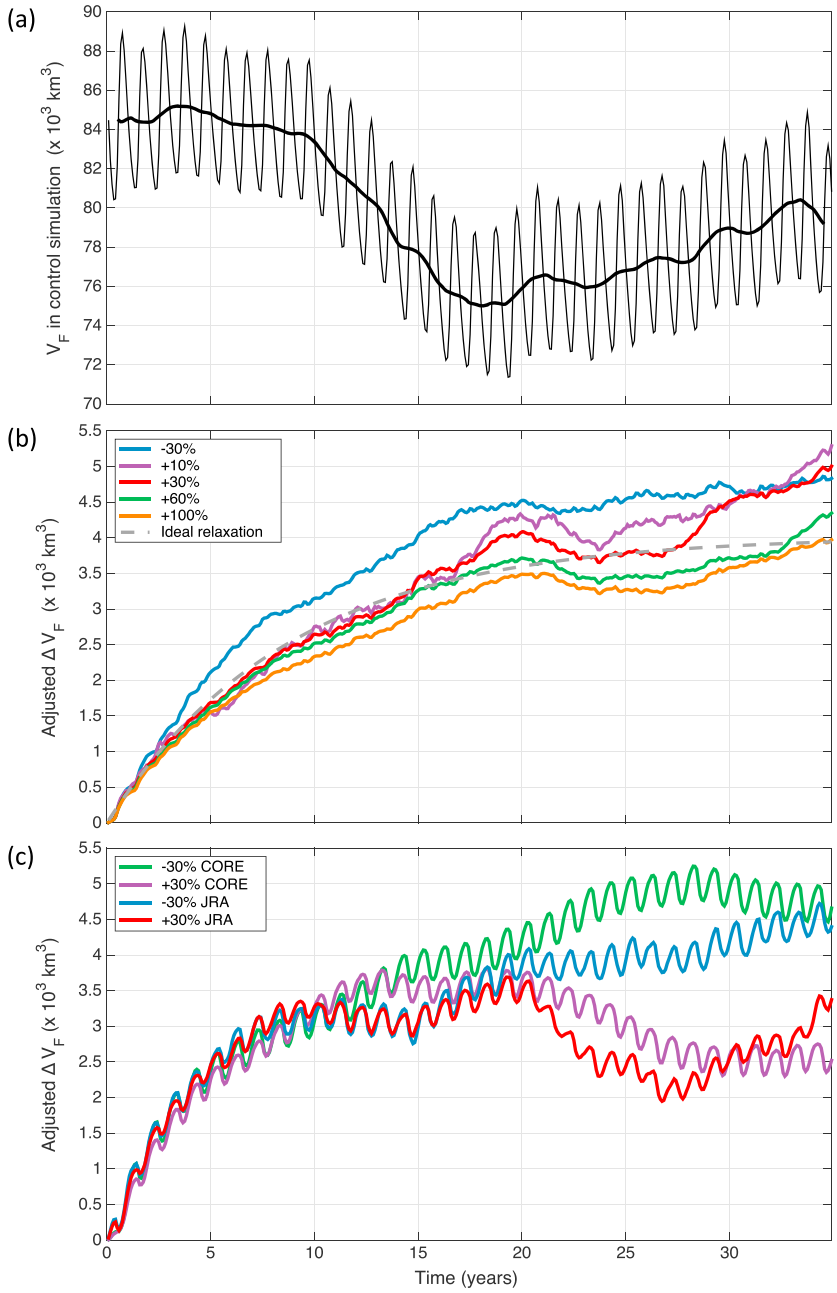

Figure 4. Time evolution in years of (a) V_F in the reference simulation; (b) anomaly of V_F with respect to the reference simulation in the simulations involving perturbation of river runoff; and (c) anomaly of V_F with respect to the reference simulation in the simulations involving perturbation of precipitation. In (a), monthly mean V_F is shown by the thinner black line, while the heavier line denotes a 12-month running mean. In (b), the solid lines indicate V_F anomalies resulting from runoff perturbations as indicated in the panel, normalized by the proportionate size of the perturbation to be equivalent to a 30% increase. The dashed gray line represents an averaged ideal exponential evolution fitted to the first 10 years of the simulations. In (c), the blue and red solid lines relate to simulations forced, as for the runoff simulations, with JRA-25 data, while the green and purple lines relate to the equivalent simulations using CORE-II forcing, which has an annual cycle but no interannual variability. As in (b), negative anomalies from experiments involving decreased freshwater input have been flipped to the positive *y* axis. CORE = Coordinated Ocean-Ice Reference Experiments; JRA-25 = Japanese 25-year Reanalysis.

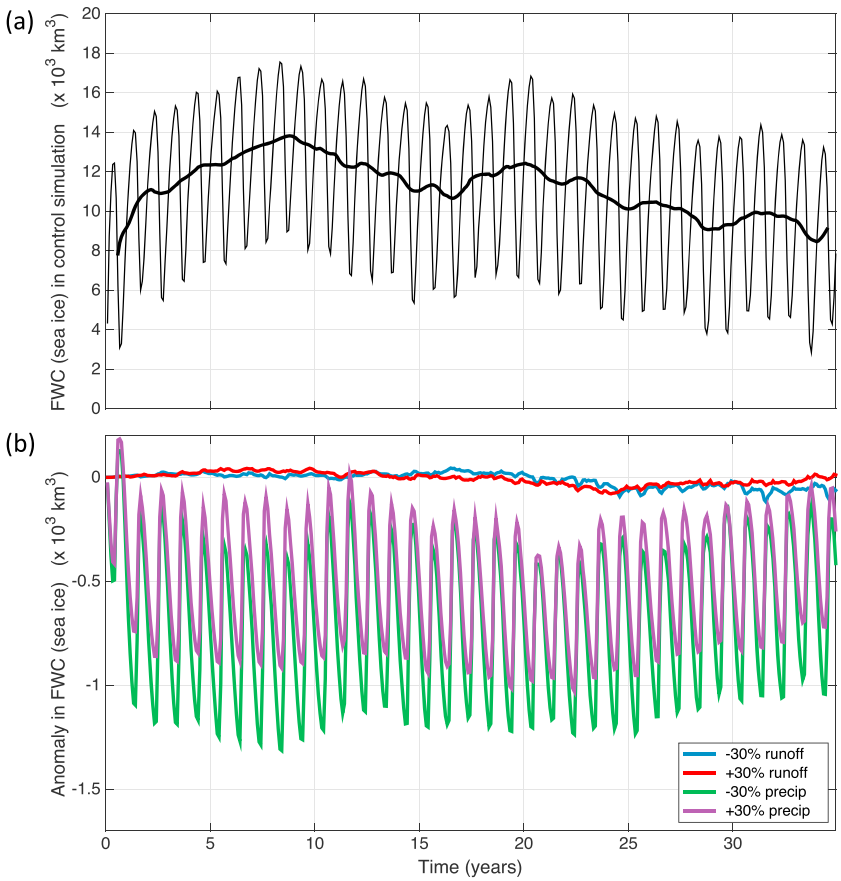

Figure 5. Time evolution in years of (a) sea ice FWC in the reference simulation; (b) anomaly of sea ice FWC with respect to the reference simulation in the simulations involving perturbation by ±30% of river runoff or precipitation. In (a), monthly mean FWC is shown by the thinner black line, while the heavier line denotes a 12-month running mean. In (b), anomalies from experiments involving decreased freshwater input have been flipped on the *y* axis. FWC = freshwater content.

3.2. Runoff

Figure 4b shows the evolving anomaly in liquid FWC relative to the control for the series of simulations involving perturbed river runoff. Values for the anomalies are normalized by the sign and scale of perturbation to a 30% increase, that is to say, $\Delta V_{\mathrm{F}} = (V_{\mathrm{F(expt)}} - V_{\mathrm{F(control)}}) \times (30\%/\text{percentage increase in runoff})$.

As expected, a decrease in freshwater input results in a negative anomaly in V_{F} compared to the control, while increases generate positive anomalies. The anomaly is close to proportional in magnitude to the perturbation of freshwater input, even for comparatively large perturbations. However, there is some asymmetry between negative and positive perturbations, and larger increases in runoff lead to proportionally slightly smaller increases in V_{F} anomaly, implying that an increasing proportion of the added freshwater is exported from the Arctic as freshwater input increases. In contrast to the precipitation experiments described below, except in the earliest years of the simulations, when a signal of the strongly seasonal river input can be detected, no annual cycle is apparent in the anomalies. Anomalies in sea ice volumes (Figure 5b) are negligible, indicating that perturbation of freshwater input through river runoff has minimal effect on the seasonal storage of freshwater in sea ice. This is consistent with the linear freshwater dynamics described by equation (14), which act as a low-pass filter: The seasonal change of the freshwater forcing is reduced roughly by a factor $\tau_{\mathrm{year}}/\tau$ relative to time mean change (see equation (5) and the ensuing discussion in Marshall et al., 2017), where τ_{year} is a year divided by 2π. Taking $\tau \sim 10$ years and $\tau_{\mathrm{year}} \sim 1/(2\pi)$ years gives an amplitude of the seasonally varying response that is only a few percent of the time mean response.

The 35-year period of integration is not sufficiently long for a new equilibrium to be reached in each simulation, but we see that the adjustment is to first-order exponential. The mean time scale, calculated by fitting

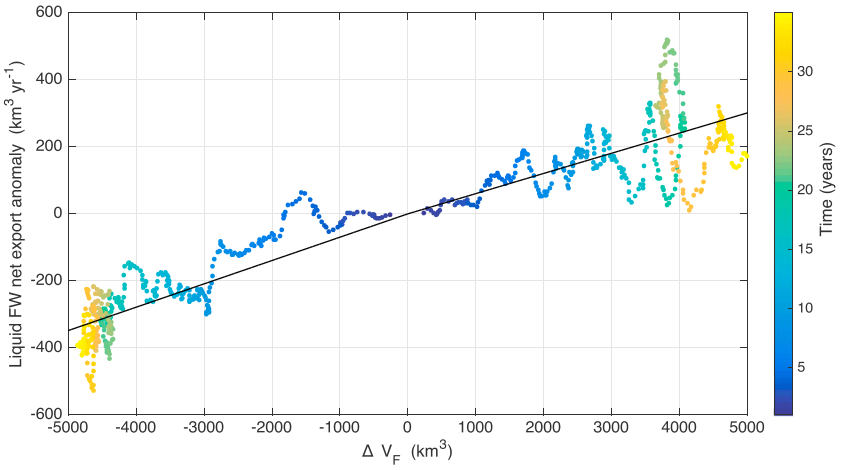

Figure 6. Anomaly in combined net export of freshwater (12-month running mean) through the straits marked in Figure 1, as a function of anomaly in liquid freshwater content for simulations involving a 30% increase and decrease in river runoff. The evolution of anomalies with time is shown by the color coding. The black lines are fitted by robust regression using an iteratively reweighted least squares model. The inverse slope of each fitted line gives a time scale, which is 17 years for increasing runoff and 14 years for decreasing runoff.

an exponential curve to anomalies for the first 10 years of the simulations, is about 9 years; it is shown by the gray dashed line in Figure 4b.

For the response to change in freshwater input to exhibit the linearity predicted by the conceptual model of Stigebrandt (1981), Nilsson and Walin (2010), and Rudels (2010), we would expect to see a direct proportionality between anomaly in V_F and anomaly in export of freshwater. A comparison for the runoff experiments is shown in Figure 6. Initially, there is indeed a good linear fit between V_F and export anomalies in both the positive and negative simulations. Further into the experiments, however, the coupling becomes less pronounced, and in the final decade especially, we see a range of possible export anomalies for a given anomaly in V_F. A straight line fit provides a further estimated time scale: 17 years for the positive simulation and 14 years in the negative case. The longer adjustment time scales obtained for the whole simulation period suggest the presence of two time scales: a faster initial exponential one and a second slower one tied to the residual variations of the freshwater anomaly. As discussed below, the deviation from a simple exponential adjustment is more pronounced for the response to precipitation changes.

3.3. Precipitation

An underlying exponential form is also apparent in the response to perturbation of precipitation, with simulations involving a decrease and an increase of precipitation by 30% shown by the blue and red lines in Figure 4c. The slight asymmetry between positive and negative perturbations that was seen in the case of river runoff is absent in the precipitation simulations, at least in the first 15 years of the simulation period. In the latter part of the period, however, there is some decadal-scale variability that is more pronounced than that for runoff and affects the responses to increases and decreases in precipitation differently. This is discussed further below.

In contrast to the runoff experiments, some residual seasonal cycle is evident in the precipitation anomalies that is accompanied by compensating seasonality in anomalies in freshwater storage in sea ice (Figure 5b). The seasonal cycle in the anomalies in liquid FWC, ΔV_F, is in antiphase with the cycle in the absolute volumes in the reference case and experiments; this indicates that increasing precipitation *depresses* the seasonal cycle and vice versa. To the extent that the extra precipitation falls as snow, our result is consistent with findings reported in the literature (Notz, 2009) that increasing snowfall over sea ice increases the thermal insulation provided by the ice, inhibiting the exchange of heat between ocean and atmosphere and thus the annual freeze and melt of sea ice. The amplitude of the residual seasonal cycle seen in the freshwater anomalies is slightly greater for negative perturbation of precipitation than for positive: of the order of 500 km^3 as opposed to 400 km^3. One would expect to see such asymmetry if changing snow cover is the cause, since a reduction in snowfall would be expected to produce a greater proportionate change in overall snow thickness than an increase of the same magnitude.

In the latter half of the period, as mentioned above, the response to perturbation of precipitation is less clean than that to changing runoff. The more pronounced variability over interannual and decadal time scales apparent in the evolution of ΔV_F is only in small part accounted for by variation in annual mean sea ice freshwater storage. As we discussed in section 2.3, changes in the storage of freshwater in the Beaufort Gyre are known to be associated with variation in atmospheric circulation over these time scales (several authors, summarized by Haine et al., 2015). We have therefore investigated whether the variability in ΔV_F might derive from the historical interannual variability in the JRA-25 reanalysis wind forcing by rerunning the precipitation simulations with the climatological CORE-II forcing, which lacks interannual variability. Anomalies in V_F from these further simulations are shown in green and purple in Figure 4c. Some of the variability between 1989 and 1994, a period dominated by cyclonic atmospheric circulation, is eliminated, but a notable divergence in behavior in the positive and negative simulations is still apparent in the years 1998 to 2002. In the simulations involving increased precipitation, ΔV_F declines at this time because of enhanced export of freshwater through the Fram Strait. This coincides with the appearance of a region of enhanced freshwater height, H_F, to the north of Greenland and just upstream of the Fram Strait. No corresponding salinity anomaly or reduction in freshwater export is seen in the freshwater decrease experiments.

4. Discussion

A necessary condition for the applicability of the CRF methodology is a linear relationship between applied forcing and observed response. The results of the simulations presented in section 3 demonstrate that this condition is well met, at least for the runoff simulations. We find that the CRF for the response of Arctic Ocean FWC to a perturbation of river runoff approximates to an exponential equilibration with a time scale of about 10 years. This figure accords with the bulk residence time (freshwater volume divided by rate of inflow) for Eurasian runoff of 10 years determined by Pemberton et al. (2014) using tracer simulations and is in line with the comparator studies they quote, including Jahn et al. (2010).

The 10-year time scale of the CRF estimated from our simulations also corresponds reasonably well to the 12- to 16-year estimates implied by the two-layer conceptual model for geostrophically controlled outflow (see equations (17) and (18)). As equation (19) indicated, were the outflow to be dominated instead by the mean background wind state, the time scale predicted by the conceptual model would be longer than seen in the simulations. Haine et al. (2015) found that such a geostrophic model, when forced with observed variations in freshwater supply, had only limited skill in explaining observed changes in Arctic Ocean FWC. Their results—and those we report here (see Figure 4a)—suggest that the observed changes were driven by wind variations rather than by changes in freshwater input. (Even if outflow is not controlled by the long-term mean wind state, its time-varying component may still be significant.) Consequently, the observed evolution of the FWC is expected to be controlled, primarily, by the forcing history of winds over the Arctic and their associated CRFs (Johnson et al., 2018). However, the current simulations have been designed to isolate CRFs for freshwater input, which illuminate different aspects of Arctic freshwater dynamics.

The first effects of changed freshwater input appear rapidly in the anomalies of freshwater export. A purely exponential CRF would require freshwater export to respond immediately to changes in input, but in the real ocean, we would of course expect a delay to allow a signal to be transmitted from the main input regions—the Siberian and Mackenzie River outflows in the case of runoff—to the export straits many hundreds of kilometers away. We have estimated the minimum time required for water of altered salinity to be advected from the Siberian shelf to the Fram Strait by tracking salinity anomalies in the model along the Transpolar Drift. This is the most direct route and one along which higher than average current speeds are typically seen (see, e.g., Pemberton & Nilsson, 2016, Figure 3). Our estimates average about 4 years. Inspection of the transient V_F anomalies shown in Figure 4b, however, reveals some curvature, implying that freshwater exports start to respond and partially offset the perturbation of freshwater input, within the first 4 years of the simulations. An early evolution of export anomalies is also apparent in Figure 6, particularly for the simulation involving increasing runoff. It is not possible to attribute these early export anomalies conclusively to a response to changing freshwater input, but our results do provide an indication of a response in exports that is triggered faster than an advection signal could be transmitted. Enhancements in freshwater export can have two possible causes: anomalously low salinity in the water flowing out through the straits and an increase in the volumetric export of water of unchanged salinity. The first cannot explain the early changes in export, since salinity anomalies cannot travel faster than advection speed; however, the second could, if

changes in freshwater input in the basin generated a dynamical signal that changed the outflow velocity at the borders of the Arctic. This might propagate as a baroclinic Kelvin wave. Assuming a mode 1 baroclinic Rossby radius, a_1, of 10 km (Nurser & Bacon, 2014) and a Coriolis parameter, f, of 1.4×10^{-4} s^{-1}, the propagation speed of such a wave, given by $c_1 = a_1 f$ (Gill, 1982), would be 1.4 m/s, allowing it to circumnavigate the Arctic basin in about 60 days.

While the underlying form of the transient responses to changing runoff and precipitation is the same, there are also some differences which could offer some pointers to the processes responsible for deviations from the first-order exponential form of the CRFs. A seasonal signal in V_F anomaly due to changes to sea ice growth is apparent only in the precipitation simulations, which exhibit more marked variability over decadal scales than those involving perturbation of runoff. Could it be, therefore, that variability in liquid freshwater storage is linked to changing storage of freshwater in sea ice form? Analysis of sea ice volumes in the precipitation experiments (Figure 5b) shows that this is not the case. After rapid adjustment over the first 2 to 3 years, anomalies in seasonally averaged sea ice freshwater storage remain largely constant over the simulation period, and the annual mean anomalies do not, at any point, increase beyond 700 km^3 in magnitude for an increase in precipitation and 800 km^3 for a decrease. This is smaller than the 1,300 km^3 by which the anomaly in liquid freshwater storage decreases between years 20 and 27 in the simulation of increasing precipitation, indicating that the temporary shortfall in liquid freshwater cannot be accounted for entirely by storage in sea ice.

The influence of changing wind patterns on V_F in the control simulation (Figure 4a) leads us to consider whether, alternatively, the variation in freshwater anomalies could be wind-driven. We note some departure from exponential form between years 10 and 18 in the JRA-25 forced simulations which is not reproduced in those forced with the climatological wind fields. This coincides with the rapid discharge in the control simulation; it is accompanied by enhanced net freshwater exports in the precipitation increase experiments and depressed exports in the decrease experiments. In the terms of the conceptual model described in section 2.3, the variability in FW export is consistent with a nonnegligible variation ($\Delta v(t)$) in wind-driven export flow (see equation (13)). This would be expected initially to retard the growth in magnitude of the freshwater height anomaly, ΔH_F; a decrease in background freshwater height, H_F, would then cause the geostrophically driven component of freshwater export to decline, partially compensating for the increase in wind-driven flow. Nevertheless, the more pronounced variability seen over the following decade is common to both the simulations employing the observationally based, interannually varying JRA-25 forcing and those using the CORE-II climatology. This indicates that winds are not the primary cause of the variability and that we must again look elsewhere for an explanation.

As we showed in section 3.3, enhanced export of freshwater through the Fram Strait in the positive precipitation experiment between years 19 and 23 was accompanied by the appearance of a region of enhanced H_F just upstream of the strait. This leads us to consider a final hypothesis for the cause of the second order form of the V_F responses, which is suggestive of a secondary time scale: That it is due to the advection of salinity anomalies from source regions to the borders of the Arctic, where they lead to variability in freshwater export. Some further insight may be gained by inspection of the evolving spatial variability in ΔV_F. Figure 7 shows time mean ΔV_F for the first and last decades of the JRA-25-forced simulations. Pemberton and Nilsson (2016) noted both the profound effect on freshwater height north of the CAA and Greenland, and the changes in the circulation and location of the Beaufort Gyre, that perturbation of freshwater input could generate. We observe from Figure 7 that these effects arise with differing time scales.

In the early stages of the runoff simulations (Figures 7a and 7c), we see an increase and decrease in freshwater height in response to increasing and decreasing runoff, respectively, that are largely confined to the Siberian shelves where the bulk of the freshwater input occurs; later in the simulations (Figures 7e and 7g), a salinity signal is seen to spread along the main advection pathways. Marshall et al. (2017) had observed that the FWC of the Beaufort Gyre is insensitive to an increase in river runoff, even when it is 3 times the size of the largest we have introduced here. They inferred that most of the extra freshwater, rather than being accumulated in the Gyre, is transported via the Transpolar Drift to the Fram and Canadian straits. Our simulation shows that ultimately much of the increase in freshwater height is seen upstream of these straits, supporting the conclusion of Marshall et al. (2017). In contrast, in computing the CRF for the FWC of the Arctic basin as a whole, we find that sufficient freshwater is retained in other areas of the Arctic Ocean not

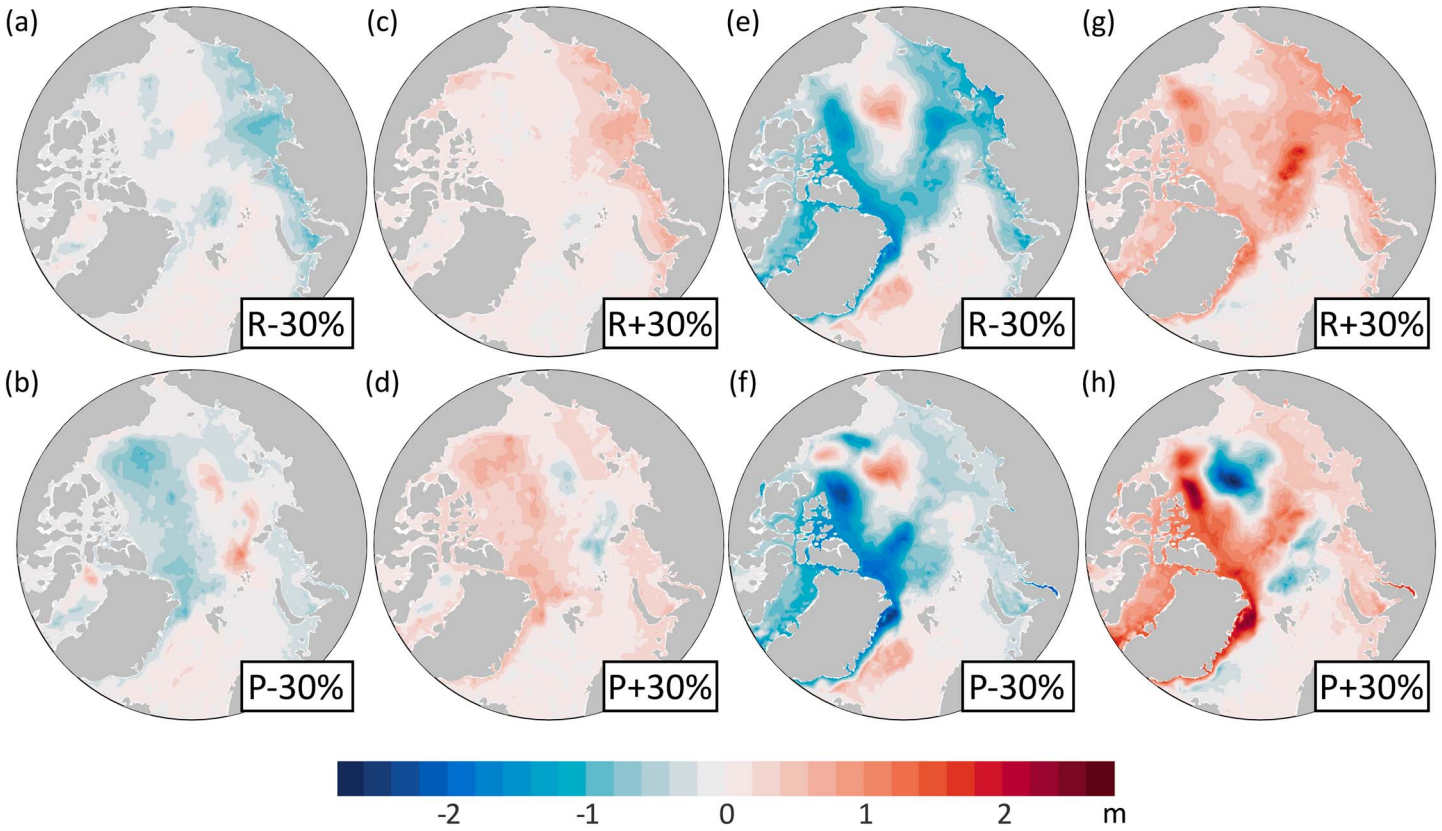

Figure 7. Anomaly in freshwater height for simulations involving increases and decreases of river runoff and precipitation of 30%. (a) to (d) show time means for the first 10 years; (e) to (h) show time means for the last 10 years (colormap from cmocean, Thyng et al., 2016).

subject to large variability in storage conditions to show exponential relaxation toward a new, elevated level of FWC.

This finding has implications for predictions of the effect on freshwater storage of future changes to wind patterns, both those driving Ekman pumping in the Beaufort Gyre region and those in the vicinity of the Arctic straits which control the local currents exporting freshwater from the Arctic. Increasing freshwater input is expected to change the distribution of the freshwater pool on which those winds will act, shifting freshwater away from the Gyre and toward the main export straits.

The largest future change projected for the Arctic Ocean freshwater budget is reduced sea ice export (Holland et al., 2007). Although we have not perturbed sea ice formation directly in the current simulations, we note that observed reduction in new ice formation has a large signal over the Siberian shelf (Comiso, 2012). We would expect, therefore, that the footprint of the response of liquid freshwater to declining sea ice formation will be similar to that of river runoff.

In the precipitation simulations, anomalies in freshwater height are seen in the early years in the Barents and Kara seas where precipitation is the highest and the perturbations thus have the greatest magnitude; however, more pronounced changes are apparent across much of the Canada Basin and the region to the north of Greenland, areas where less precipitation occurs but sea ice tends to be the thickest. The rapid appearance of anomalies in this area contrasts with the runoff experiments, where the early response was limited to the freshwater source regions. The pattern of the precipitation response accords with Pemberton and Nilsson (2016), who found that a decrease in precipitation ultimately leads to an increase in sea ice thickness north of Greenland. As the salinity anomalies accumulating in these regions due to interactions with sea ice are advected through the various export straits just to the south, they would be expected to lead to the variability in freshwater exports visible in Figure 6. They can thus explain several of the features seen in the CRFs, including the slight decline in ΔV_F after 10–15 years in Figure 4c and the more pronounced declines in the latter part of the simulation period.

A further potential source of complexity in the response is the time scale associated with alteration of the major Arctic circulation pathways. Pemberton and Nilsson (2016) found that increasing freshwater input leads to a decrease in the strength of the Beaufort Gyre circulation and a shift in export from the CAA to the Fram Strait; Figure 7 shows that indications of these changes in the form of altered freshwater storage in the region of the Gyre are apparent only in the later years of the simulations.

5. Conclusions

We have investigated the transient response of FWC in the Arctic Ocean to changing freshwater input, comparing the effects of perturbation of river runoff and precipitation. We offer a CRF for river runoff, which takes the form of a simple exponential relaxation with a time scale of approximately 10 years. This agrees with the predictions of a simple two-layer conceptual model for rotationally controlled export of freshwater. Although to first order sharing the exponential form of the runoff response, the response to changing precipitation shows additional complexity consistent with a secondary time scale. We suggest that this is due in part to the greater importance of ocean-ice interactions in the precipitation case; these give rise to localized salinity anomalies which cause variability in freshwater exports when they are advected through the straits at the boundaries of the Arctic. Regardless of the source of freshwater input, the response is largely independent of the wind-forcing regime over the Arctic Ocean.

Our results suggest that the fate of enhanced freshwater input to the Arctic and the proportion of extra freshwater stored within the Arctic rather than being discharged immediately to the subpolar seas depend on the mode and footprint of this input. Although river runoff is projected to contribute a greater share of future increases in freshwater input than is precipitation, we find that runoff produces a simpler transient response in terms of storage and export of freshwater. In the case of precipitation, a greater proportion of the supplied freshwater enters regions of the Arctic where interactions between the freshwater anomalies and the sea ice and the mean circulation are more complicated. As a result, the transient response of the freshwater storage to changes in precipitation is more complex than that related to changes in runoff. Such is the importance of nonlinear interactions between the ocean and sea ice in the precipitation response that accurate projections of the effect of future increases in precipitation will require models that can capture ice-ocean interactions well.

Acknowledgments
N. J. B. was supported by the UK Natural Environmental Research Council (Grant NE/L002531/1). J. N. acknowledges the support of the Swedish National Space Board. P. P. is funded by NordForsk project Nordic Center of Excellence Arctic Climate Prediction: Pathways to Resilient, Sustainable Societies (ARCPATH), Grant 76654. The model output used in the analysis described in this paper is available online (http://doi.org/10.5281/zenodo.2648763). Analysis scripts can be found online (https://github.com/njb1n12/Arctic-freshwater). The authors are grateful to Andrey Proshutinsky and to the Editor and two anonymous reviewers whose comments greatly improved the paper.

References

Antonov, J. I., Locarnini, R. A., Boyer, T. P., Mishonov, A. V., & Garcia, H. E. (2006). World Ocean Atlas 2005, volume 2: Salinity. In S. Levitus (Ed.), *NOAA Atlas NESDIS 62*. Washington, DC: U.S. Government Printing Office.

Bintanja, R., & Selten, F. M. (2014). Future increases in Arctic precipitation linked to local evaporation and sea-ice retreat. *Nature*, *509*(7501), 479–482. https://doi.org/10.1038/nature13259

Comiso, J. C. (2012). Large decadal decline of the Arctic multiyear ice cover. *Journal of Climate*, *25*(4), 1176–1193. https://doi.org/10.1175/JCLI-D-11-00113.1

Condron, A., Winsor, P., Hill, C., & Menemenlis, D. (2009). Simulated response of the Arctic freshwater budget to extreme NAO wind forcing. *Journal of Climate*, *22*(9), 2422–2437. https://doi.org/10.1175/2008jcli2626.1

Dewey, S., Morison, J., Kwok, R., Dickinson, S., Morison, D., & Andersen, R. (2018). Arctic ice-ocean coupling and gyre equilibration observed with remote sensing. *Geophysical Research Letters*, *45*, 1499–1508. https://doi.org/10.1002/2017gl076229

Eldevik, T., & Nilsen, J. E. O. (2013). The Arctic-Atlantic thermohaline circulation. *Journal of Climate*, *26*(21), 8698–8705. https://doi.org/10.1175/JCLI-D-13-00305.1

Gill, A. (1982). *Atmosphere-ocean dynamics*. San Diego, CA: Academic Press.

Griffies, S. M., Biastoch, A., Boning, C., Bryan, F., Danabasoglu, G., Chassignet, E. P., et al. (2009). Coordinated Ocean-ice Reference Experiments (COREs). *Ocean Modelling*, *26*(1-2), 1–46. https://doi.org/10.1016/j.ocemod.2008.08.007

Haine, T. W. N., Curry, B., Gerdes, R., Hansen, E., Karcher, M., Lee, C., et al. (2015). Arctic freshwater export: Status, mechanisms, and prospects. *Global and Planetary Change*, *125*, 13–35. https://doi.org/10.1016/j.gloplacha.2014.11.013

Held, I. M., & Soden, B. J. (2006). Robust responses of the hydrological cycle to global warming. *Journal of Climate*, *19*(21), 5686–5699. https://doi.org/10.1175/Jcli3990

Holland, M. M., Finnis, J., Barrett, A. P., & Serreze, M. C. (2007). Projected changes in Arctic Ocean freshwater budgets. *Journal of Geophysical Research*, *112*, G04S55. https://doi.org/10.1029/2006JG000354

Jahn, A., Tremblay, L. B., Newton, R., Holland, M. M., Mysak, L. A., & Dmitrenko, I. A. (2010). A tracer study of the Arctic Ocean's liquid freshwater export variability. *Journal of Geophysical Research*, *115*, C07015. https://doi.org/10.1029/2009JC005873

Johnson, H. L., Cornish, S. B., Kostov, Y., Beer, E., & Lique, C. (2018). Arctic Ocean freshwater content and its decadal memory of sea-level pressure. *Geophysical Research Letters*, *45*, 4991–5001. https://doi.org/10.1029/2017GL076870

Lambert, E., Nummelin, A., Pemberton, P., & Ilicak, M. (2019). Tracing the imprint of river runoff variability on Arctic water mass transformation. *Journal of Geophysical Research: Oceans*, *124*, 302–319. https://doi.org/10.1029/2017jc013704

Locarnini, R. A, Mishonov, A. V., Antonov, J. I., Boyer, T. P., & Garcia, H. E. (2006). World Ocean Atlas 2005, volume 1: Temperature. In S. Levitus (Ed.), *NOAA Atlas NESDIS 61*. Washington, DC: U.S. Government Printing Office.

Manizza, M., Follows, M. J., Dutkiewicz, S., McClelland, J. W., Menemenlis, D., Hill, C. N., et al. (2009). Modeling transport and fate of riverine dissolved organic carbon in the Arctic Ocean. *Global Biogeochemical Cycles*, *23*, GB4006. https://doi.org/10.1029/2008gb003396

Manucharyan, G. E., & Spall, M. A. (2016). Wind-driven freshwater buildup and release in the Beaufort Gyre constrained by mesoscale eddies. *Geophysical Research Letters*, *43*, 273–282. https://doi.org/10.1002/2015gl065957

Marshall, J., Scott, J., & Proshutinsky, A. (2017). "Climate response functions" for the Arctic Ocean: A proposed coordinated modelling experiment. *Geoscientific Model Development*, *10*(7), 2833–2848. https://doi.org/10.5194/gmd-10-2833-2017

Meneghello, G., Marshall, J., Cole, S. T., & Timmermans, M. L. (2017). Observational inferences of lateral eddy diffusivity in the halocline of the Beaufort Gyre. *Geophysical Research Letters*, *44*, 12,331–12,338. https://doi.org/10.1002/2017gl075126

Morison, J., Kwok, R., Peralta-Ferriz, C., Alkire, M., Rigor, I., Andersen, R., & Steele, M. (2012). Changing Arctic Ocean freshwater pathways. *Nature*, *481*(7379), 66–70. https://doi.org/10.1038/nature10705

Nguyen, A. T., Menemenlis, D., & Kwok, R. (2011). Arctic ice-ocean simulation with optimized model parameters: Approach and assessment. *Journal of Geophysical Research*, *116*, C04025. https://doi.org/10.1029/2010JC006573

Nilsson, J., & Walin, G. (2010). Salinity-dominated thermohaline circulation in sill basins: Can two stable equilibria exist? *Tellus Series A-Dynamic Meteorology and Oceanography*, *62*(2), 123–133. https://doi.org/10.1111/j.1600-0870.2009.00428.x

Notz, D. (2009). The future of ice sheets and sea ice: Between reversible retreat and unstoppable loss. *Proceedings of the National Academy of Sciences of the United States of America*, *106*(49), 20,590–20,595. https://doi.org/10.1073/pnas.0902356106

Nummelin, A., Ilicak, M., Li, C., & Smedsrud, L. H. (2016). Consequences of future increased Arctic runoff on Arctic Ocean stratification, circulation, and sea ice cover. *Journal of Geophysical Research: Oceans*, *121*, 617–637. https://doi.org/10.1002/2015jc011156

Nurser, A. J. G., & Bacon, S. (2014). The Rossby radius in the Arctic Ocean. *Ocean Science*, *10*(6), 967–975. https://doi.org/10.5194/Os-10-967-2014

Onogi, K., Tslttsui, J., Koide, H., Sakamoto, M., Kobayashi, S., Hatsushika, H., et al. (2007). The JRA-25 reanalysis. *Journal of the Meteorological Society of Japan*, *85*(3), 369–432. https://doi.org/10.2151/jmsj.85.369

Pemberton, P., & Nilsson, J. (2016). The response of the central Arctic Ocean stratification to freshwater perturbations. *Journal of Geophysical Research: Oceans*, *121*, 792–817. https://doi.org/10.1002/2015jc011003

Pemberton, P., Nilsson, J., & Meier, H. E. M. (2014). Arctic Ocean freshwater composition, pathways and transformations from a passive tracer simulation. *Tellus Series A-Dynamic Meteorology and Oceanography*, *66*, 23988. https://doi.org/10.3402/tellusa.v66.23988

Polyakov, I. V., Alexeev, V. A., Belchansky, G. I., Dmitrenko, I. A., Ivanov, V. V., Kirillov, S. A., et al. (2008). Arctic Ocean freshwater changes over the past 100 years and their causes. *Journal of Climate*, *21*(2), 364–384. https://doi.org/10.1175/2007JCLI1748.1

Proshutinsky, A., Dukhovskoy, D., Timmermans, M. L., Krishfield, R., & Bamber, J. L. (2015). Arctic circulation regimes. *Philosophical Transactions of the Royal Society a-Mathematical Physical and Engineering Sciences*, *373*(2052), 20140160. https://doi.org/10.1098/rsta.2014.0160

Proshutinsky, A., Krishfield, R., Timmermans, M. L., Toole, J., Carmack, E., McLaughlin, F., et al. (2009). Beaufort Gyre freshwater reservoir: State and variability from observations. *Journal of Geophysical Research*, *114*, C00A10. https://doi.org/10.1029/2008JC005104

Proshutinsky, A. Y., Polyakov, I. V., & Johnson, M. A. (1999). Climate states and variability of Arctic ice and water dynamics during 1946–1997. *Polar Research*, *18*(2), 135–142. https://doi.org/10.1111/j.1751-8369.1999.tb00285.x

Rabe, B., Karcher, M., Schauer, U., Toole, J. M., Krishfield, R. A., Pisarev, S., et al. (2011). An assessment of Arctic Ocean freshwater content changes from the 1990s to the 2006–2008 period. *Deep-Sea Research Part I-Oceanographic Research Papers*, *58*(2), 173–185. https://doi.org/10.1016/j.dsr.2010.12.002

Rudels, B. (2010). Constraints on exchanges in the Arctic mediterranean—Do they exist and can they be of use? *Tellus Series A-Dynamic Meteorology and Oceanography*, *62*(2), 109–122. https://doi.org/10.1111/j.1600-0870.2009.00425.x

Rudels, B., Schauer, U., Bjork, G., Korhonen, M., Pisarev, S., Rabe, B., & Wisotzki, A. (2013). Observations of water masses and circulation with focus on the Eurasian Basin of the Arctic Ocean from the 1990s to the late 2000s. *Ocean Science*, *9*(1), 147–169. https://doi.org/10.5194/Os-9-147-2013

Stewart, K. D., & Haine, T. W. N. (2013). Wind-driven Arctic freshwater anomalies. *Geophysical Research Letters*, *40*, 6196–6201. https://doi.org/10.1002/2013gl058247

Stigebrandt, A. (1981). A model for the thickness and salinity of the upper layer in the Arctic Ocean and the relationship between the ice thickness and some external parameters. *Journal of Physical Oceanography*, *11*(10), 1407–1422. https://doi.org/10.1175/1520-0485(1981)011<1407:AMFTTA>2.0.CO;2

Thyng, K. M., Greene, C. A., Hetland, R. D., Zimmerle, H. M., & DiMarco, S. F. (2016). True colors of oceanography guidelines for effective and accurate colormap selection. *Oceanography*, *29*(3), 9–13. https://doi.org/10.5670/oceanog.2016.66

Vavrus, S. J., Holland, M. M., Jahn, A., Bailey, D. A., & Blazey, B. A. (2012). Twenty-first-century Arctic climate change in CCSM4. *Journal of Climate*, *25*(8), 2696–2710. https://doi.org/10.1175/Jcli-D-11-00220.1

Woodgate, R. A., Aagaard, K., Swift, J. H., Falkner, K. K., & Smethie, W. M. (2005). Pacific ventilation of the Arctic Ocean's lower halocline by upwelling and diapycnal mixing over the continental margin. *Geophysical Research Letters*, *32*, L18609. https://doi.org/10.1029/2005GL023999

Yang, Q., Dixon, T. H., Myers, P. G., Bonin, J., Chambers, D., van den Broeke, M. R., et al. (2016). Recent increases in Arctic freshwater flux affects Labrador Sea convection and Atlantic overturning circulation. *Nature Communications*, *7*, 10525. https://doi.org/10.1038/ncomms10525

Zhang, J. L., & Rothrock, D. A. (2003). Modeling global sea ice with a thickness and enthalpy distribution model in generalized curvilinear coordinates. *Monthly Weather Review*, *131*(5), 845–861. https://doi.org/10.1175/1520-0493(2003)131<0845:MGSIWA>2.0.CO;2